Visually evoked activity in cortical cells imaged in freely moving animals

Juergen Sawinski[a,1], Damian J. Wallace[a,1], David S. Greenberg[a,1], Silvie Grossmann[b], Winfried Denk[b], and Jason N. D. Kerr[a,2]

[a]Network Imaging Group, Max Planck Institute for Biological Cybernetics, Spemannstrasse 41, 72076 Tübingen, Germany; and [b]Department of Biomedical Optics, Max Planck Institute for Medical Research, Jahnstrasse 29, 69120 Heidelberg, Germany

Edited by David W. Tank, Princeton University, Princeton, NJ, and approved September 18, 2009 (received for review April 4, 2009)

We describe a miniaturized head-mounted multiphoton microscope and its use for recording Ca^{2+} transients from the somata of layer 2/3 neurons in the visual cortex of awake, freely moving rats. Images contained up to 20 neurons and were stable enough to record continuously for >5 min per trial and 20 trials per imaging session, even as the animal was running at velocities of up to 0.6 m/s. Neuronal Ca^{2+} transients were readily detected, and responses to various static visual stimuli were observed during free movement on a running track. Neuronal activity was sparse and increased when the animal swept its gaze across a visual stimulus. Neurons showing preferential activation by specific stimuli were observed in freely moving animals. These results demonstrate that the multiphoton fiberscope is suitable for functional imaging in awake and freely moving animals.

calcium imaging | head-mounted microscope | neuronal activity | two-photon | visual cortex

The observation of neural activity has been central to the vast majority of efforts to understand information processing in the mammalian brain. Although some aspects of sensory processing can be studied in animals that are anesthetized or awake but head-fixed, to fully understand awake information processing, animals must be able to interact fully with their environment. Previously, this approach, which includes both allothetic and idiothetic cues, lead to the discovery of place cells (1), head-direction cells (2), and grid cells (3). Multiphoton (MP) imaging (4) of neurons bulk-loaded with calcium indicators (5–7) allows not only the unambiguous identification and precise anatomical localization of active neurons but also the simultaneous recording of activity in multiple neurons even at very low firing rates (8–10). Although one major limitation of conventional MP imaging has been the need to firmly hold the skull in position to prevent the brain from moving relative to the microscope objective, some aspects of free movement can be simulated in head-fixed animals by placing them in a virtual reality situation (11). For measurements in truly free-moving animals, the recording apparatus must be miniaturized and attached to the skull, similar to the approach used for the recording of extracellular (1, 12) and intracellular (13) electrical signals in freely moving rodents. It is possible to use optical fibers to deliver short-pulse light suitable for two-photon excitation, scan the excitation focus, and collect the emitted fluorescence (14). There have been a number of recent advances in scanning technology (15, 16) that have been applied to anesthetized animals by using two-photon excitation (17) or freely moving animals by using one-photon wide-field imaging (18). Here we show that it is possible to use two-photon microscopy to record activity from neuronal populations with cellular resolution in freely moving animals.

Results and Discussion

We developed a fiberscope (Fig. 1*A*) that employs a custom-designed water-immersion lens and a leveraged, nonresonant fiber scanner (16), which provides greater control over the scan pattern than resonant scanning (14). Multilens objectives provide higher excitation and detection numerical apertures than gradient-index (GRIN) lenses (19), but, unlike those, do not allow deep imaging by mechanical penetration of brain tissue (20). The total weight of the head-mounted part was 5.5 g, making it well suited to be carried by adult or even adolescent rats. Emitted fluorescence is collected through a large-core, high-NA plastic optical fiber. At the fixed end of the collection fiber the fluorescence is split into a "green" channel (510–560 nm) and a "red" channel (573–648 nm), which collect fluorescence from, respectively, the calcium-indicator (Oregon green BAPTA-1, OGB1) and sulforhodamine 101 (SR101), used to selectively stain astrocytes (21). Multichannel acquisition allows ratiometric correction for fluctuations in excitation efficiency (see below), discrimination of silent neurons and astrocytes, and, in the future, the use of FRET-based indicators (22).

For transmission of the excitation beam a polarization-maintaining fiber was used to avoid excitation fluctuations due to modulations in its polarization state, which are induced by bending an ordinary fiber and which affect two-photon absorption efficiency (23). Because SR101 fluorescence is independent of neuronal activity, it can be used to normalize the green channel signal (see *Materials and Methods* and Fig. S1).

We first tested the ability of the fiberscope to detect stimulus-evoked Ca^{2+} transients in anesthetized animals (Figs. 2 *A–E*). Intrinsic optical imaging was used to locate the primary visual area responsive to stimuli presented directly in front of the animal's nose. This area was then targeted for bolus loading with OGB1-AM, and the head-mounted microscope was positioned over it (Fig. 2*A*). Spontaneous Ca^{2+}-transients (Fig. 2*B*) occurred at rates of up to 0.4 Hz (average 0.13 ± 0.03, $n = 16$ neurons, $n = 2$ animals, mean ± SEM.), consistent with previous recordings using conventional 2P-microscopy (8) in awake and extracellular recordings (24, 25) in anesthetized visual cortex. The laser power after the objective was 100–150 mW [≈40–60 mW at the focus, assuming a 200-μm scattering length (26) with an estimated pulse width of 1.8 ps (16)]. No decline of the average image intensity or any signs of cell damage were observed during the entire imaging period of >1 h. We next presented drifting gratings at four or eight different orientations ($n = 43$ and 20 neurons, respectively, $n = 2$ animals, see *Materials and Methods* for further details). Of all cells, 46% showed stimulus-evoked fluorescence increases (Fig. 2*D*, $P < 0.01$, ANOVA), and of those 72% were selective for orientation or direction (Fig. 2 *E* and *F*, $P < 0.01$, ANOVA). Neighboring neurons could have dramatically different preferences, consistent with previous findings in the rodent visual cortex (7, 24). The neuropil signal showed no direction or orientation selectivity ($P > 0.05$, ANOVA).

Author contributions: J.S., D.J.W., D.S.G., S.G., W.D., and J.N.D.K. designed research; J.S., D.J.W., and J.N.D.K. performed research; J.S., D.J.W., D.S.G., and J.N.D.K. analyzed data; and J.S., D.J.W., D.S.G., W.D., and J.N.D.K. wrote the paper.

The authors declare no conflict of interest.

This article is a PNAS Direct Submission.

Freely available online through the PNAS open access option.

See Commentary on page 19209.

[1]J.S., D.J.W., and D.S.G. contributed equally to this work.

[2]To whom correspondence should be addressed. E-mail: jason@tuebingen.mpg.de.

This article contains supporting information online at www.pnas.org/cgi/content/full/0903680106/DCSupplemental.

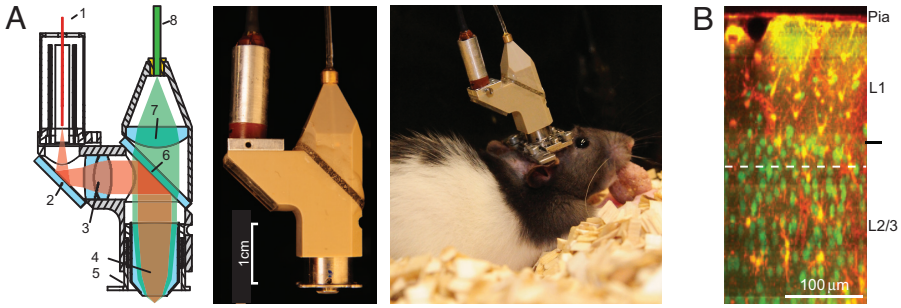

Fig. 1. Fiber optic microscope. (*A*) Schematic illustration (*Left*) showing: 1, excitation fiber (single mode); 2, folding mirror; 3, tube lens; 4, objective; 5, focusing flange; 6, beam splitter; 7, collimation lens; 8, collection fiber (multimode). Photographs showing the assembled microscope (*Center*) and the mounted microscope (*Right*). (*B*) Cortex, bulk-loaded with OGB1 and sulforhodamine 101; side-projection of an image stack acquired with a conventional MP microscope. The approximate location of the fiberscope focal plane is indicated by the dashed line.

Together these results show that the fiberscope is capable of detecting Ca^{2+} transients evoked by sensory stimulation.

To confirm that carrying the fiberscope does not impose an excessive burden on the animal, we attached it to awake and otherwise unrestrained rats. Their movements around the home cage were observed and quantified by videography under infrared illumination. The animals appeared unencumbered by the presence of the fiberscope, with normal running, digging, feeding, and pouncing behaviors throughout experimental sessions lasting up to 270 min. Distributions of velocity and acceleration were similar with (n = 5 animals, 75–100 g) and without (n = 3) the microscope (8.3 ± 7.6 vs. 9.5 ± 12.4 cm/s and 0.55 ± 0.49 vs. 0.37 ± 0.50 m/s^2, respectively, mean ± SD; see Fig. S2).

The 2P image series acquired during free movement (Fig. 3) were largely stable along all axes even while the animal was moving around the cage at velocities of up to 0.6 m/s. However, some irregular motion during chewing or vigorous head shaking occurred occasionally. Frames (≈2% of total) were excluded whenever small structures suddenly appeared or disappeared (see Fig. S3). For the remaining frames, lateral displacements were quantified by using the imaging data (16 displacements estimated per image frame) and corrected by using an algorithm described previously (27). The detected brain displacements were well within the correctable range of the motion correction algorithm (27) and were similar in amplitude and frequency of occurrence to those observed in awake head-fixed animals (8, 11). Brain displacements were weakly but significantly correlated to the animal's velocity and acceleration (Fig. S4, r = 0.25, 0.33, respectively, $P < 0.0001$, t tests, three animals, 11 imaging periods, 15,787 frames).

We next proceeded to record spontaneous and stimulus-evoked Ca^{2+} transients in freely moving animals (Movie S1). During imaging sessions, animals (n = 7) were allowed to move freely along a semicircular track. CRT monitors were positioned at each end and at the apex of the curve (Fig. 3*A*). Static visual stimuli consisting of a series of 6-cm-wide blue bars on a black background were displayed on each monitor, with the orientation of the bars being 45° and −45°, respectively, for the monitors at the track ends and vertical (0°) at the center (see *Materials and Methods* for further details). Except for the light from the monitors, all sessions were conducted in darkness, and the animals' movements on the track

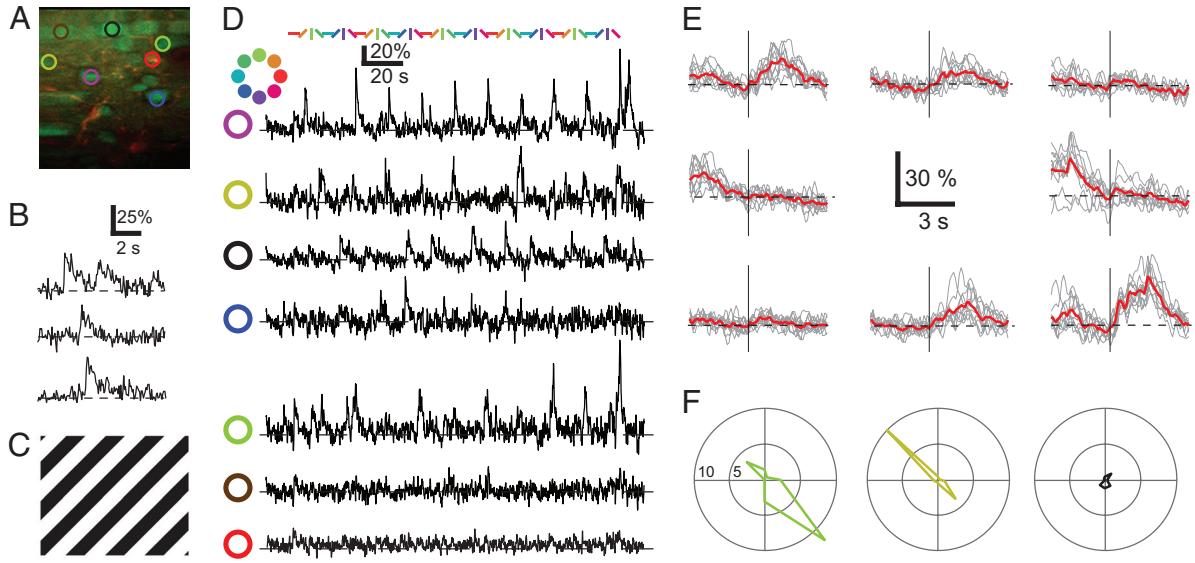

Fig. 2. Orientation tuning of neurons imaged with head-mounted microscope. (*A*) Fiberscope image (10-frame average) from an anesthetized animal, showing both neurons (green) and astrocytes (orange) in layer 2/3 of the visual cortex. (*B*) Spontaneous transients in a neuronal soma. (*C*) Moving grating as presented to the anaesthetized animal at four different orientations and two different directions. (*D*) Simultaneously recorded transients during the presentation of visual stimulation in the cell population shown in *A* (six upper traces are from neurons, lowest trace from an astrocyte; Colored bars above top trace indicate stimulus orientation). (*E*) Averaged responses (red traces) of one neuron (second trace from top in *D*) to multiple trials (gray traces) of moving gratings (trace locations correspond to movement directions). Vertical lines indicate onset of grating movement. (*F*) Direction tuning for three different neurons (same neurons as in *A* and *D* as indicated by color).

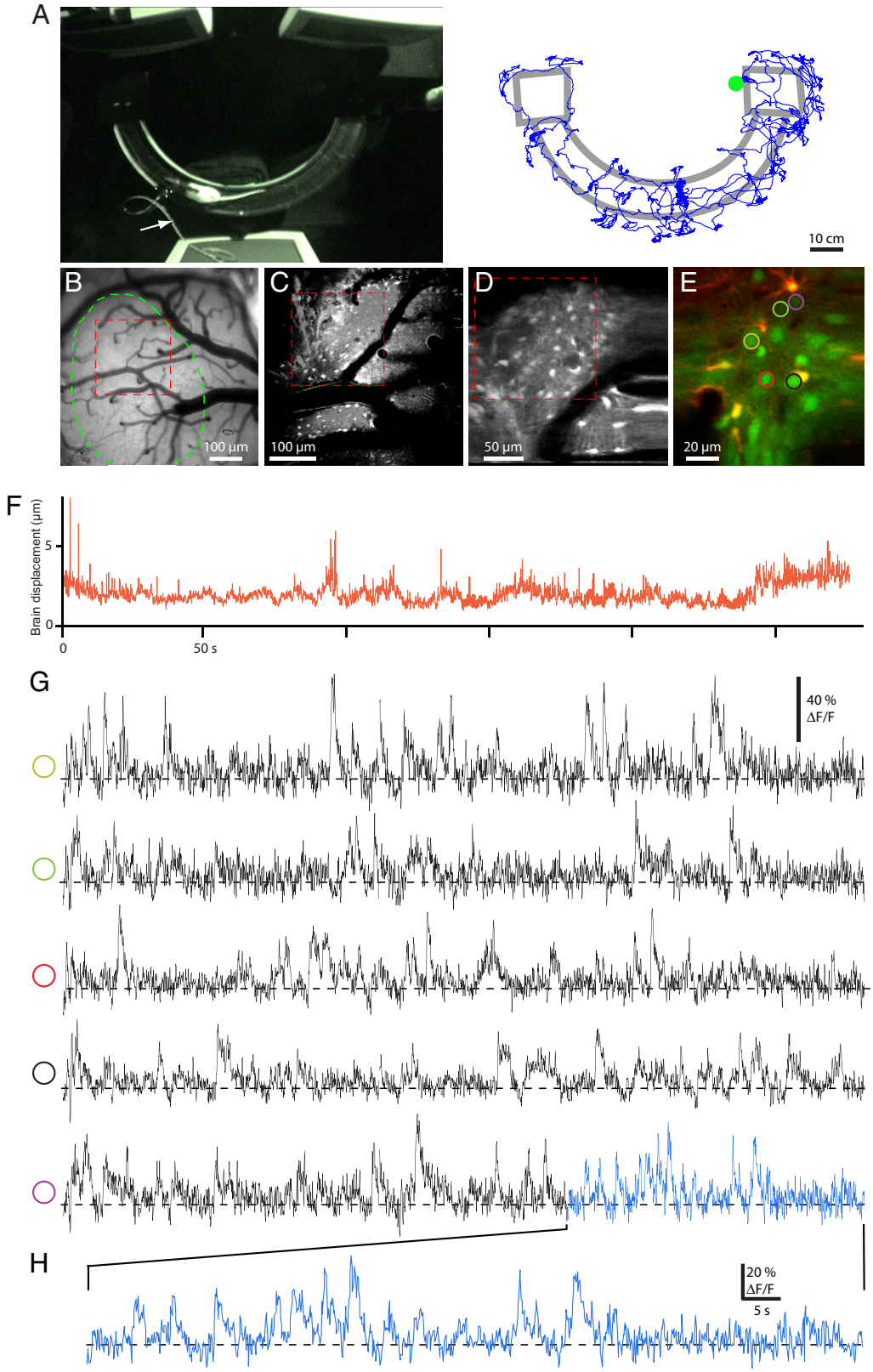

Fig. 3. Continuous imaging of activity in multiple neuronal somata in the primary visual cortex of a freely moving animal. (*A*) Overhead-camera view (fibers, arrow) and path of the animal (blue; trace starts at the green circle). Note the elevated semicircular track and the monitors used for visual stimulation. (*B–E*) Overview images (red dashed rectangles denote field of view in the following image) at the surface of the recorded area shown in *E*. Image (*B*) of the blood vessel pattern taken with a conventional camera and the approximate primary visual area identified by intrinsic imaging (green, dashed line), see *Materials and Methods* for area selection details. Surface images taken with a fixed two-photon laser scanning microscope (*C*) and with the head-mount microscope (*D*). (*E*) Two-color overlay image of the recorded area (sulforhodamine 101 channel red; OGB-1 channel green; see also Movie S1). (*F*) Brain displacement as a function of time. (*G*) Ca^{2+} time courses ($\Delta F/F_0$) in the somata of five neurons (colored circles in *E*). (*H*) A region of the trace activity magnified showing details of transients.

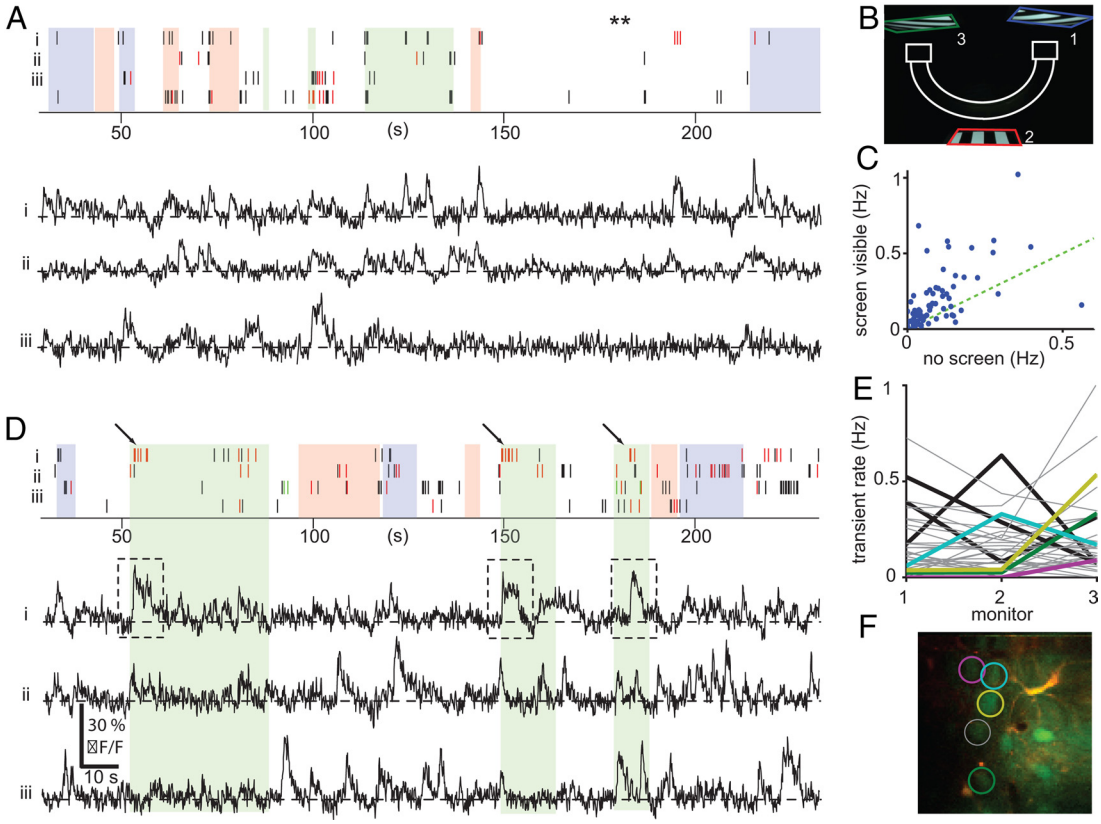

Fig. 4. Stimulus selectivity of individual neurons in a freely moving animal. (*A*) Example raster plots detailing activity in four neurons over ≈5 min of continuous recording while the animal was free to explore the elevated ramp (black lines correspond to single APs, red to doubles, and green to triples, see *SI Text* for details of the AP detection algorithm). Transients for three of the four neurons (denoted i, ii, and iii) shown below. Periods when the animal's gaze moved across one of the three monitors (shown in *B*) are indicated by the blocks of background color (color coding for the three monitors shown in *B*, see *Materials and Methods* for gaze tracking criteria). Note the long period (**) of reduced activity, beginning around 140 s, during which the animal's gaze was not on any monitor. (*C*) Grouped data from all 77 neurons ($n = 5$ animals) comparing Ca^{2+} transient frequencies with, respectively, the animal's gaze on or off any monitor. (*D*) Activity raster plot for the same neurons and the corresponding Ca^{2+} traces (below). Note multiple large transients (arrows in raster plot, dashed boxes in traces) in neuron i in response to viewing the same monitor multiple times. (*E*) Comparison of activity in 35 neurons while the animal was viewing each of the monitors in isolation (monitors labeled as in *B*). Thick lines indicate neurons with significantly enhanced responsiveness to a specific monitor. Thick colored lines refer to monitor-selective responses from the cells indicated by the circles of identical color in the image in *F*. The thin gray circle in *F* indicated a cell with no monitor preference. Note that neighboring cells can have different preferences.

were again recorded with infrared videography. As for anesthetized animals, the primary visual area representing the visual space directly in front of the animal's nose was identified by using intrinsic-signal imaging and then targeted for bolus loading with OGB-1-AM (Fig. 3 *B* and *C*). The fiberscope was again placed over the loaded area by using surface blood vessels as landmarks (Fig. 3 *D* and E). Continuous fiberscope image sequences (64 × 64 pixels, 90 ms per frame, 1.43 ms per line, Fig. 3*G*) lasting ≈5 min were recorded, with up to 18 of these sequences recorded in a single session, representing a total up to 90 min of Ca^{2+}-imaging data from the same group of neurons. All neurons displayed robust Ca^{2+}-transients (Fig. 3*G*), which were similar to action potential (AP)-induced transients measured by conventional MP microscopes in anesthetized (5, 6, 9) and awake (8, 11) animals. Transients in astrocytes were of similar amplitude (peak $\Delta F/F_0$ of 20–30%) but much slower dynamics (rise times of 2–15 s, durations of 5–100 s; Fig. S5), consistent with calcium spikes and plateaus observed in astrocytes during spontaneous activity and sensory stimulation (28).

To quantify the observed changes in neuronal activity, we applied an algorithm for automated AP detection (8) to fluorescence recorded by using the fiberscope. Because the fiberscope does not (yet) allow concurrent single-cell electrical recordings, a direct quantification of the AP detection probability and of the false-positive detection rate is not possible. However, we felt confident to apply this algorithm to the current data because the frame rates, scan-line times, look up tables (LUTs), and photon multiplier tubes (PMTs) were nearly identical to those used for its verification (8). Furthermore, when we applied the AP detection algorithm to fiberscope recordings in anesthetized animals, neither the proportion of neurons classified as visually responsive (29%) nor the proportion of these selective for stimulus angle (83%) were significantly different to those proportions determined by using $\Delta F/F_0$ values alone (see *Materials and Methods* for further details).

To further examine the relationship between the animal's movements (and, therefore, shifts in its gaze) and the simultaneously recorded Ca^{2+} transients, we first estimated the animal's position and the orientation of its head by tracking four infrared LEDs attached to the fiberscope (Movie S2). The relative orientation and distance to the animal's head were calculated for each screen by using video frames from the camera above the track. The video and Ca^{2+}-imaging traces were synchronized by using the activation of the fiberscope scanner, which was clearly visible in the infrared video frames. Individual monitors were classified as "viewed" when they subtended at least 400 square degrees inside a region extending ±45° horizontally and vertically from the forward direction (see *Materials and Methods* for details and Fig. S6). Periods when no part of any monitor was located within this region were classified as "blank." During blank periods, fewer Ca^{2+} transients were ob-

served compared to periods when the animal was moving around on the track and sweeping its gaze regularly across different monitors (Fig. 4*A*). Averaging across all neurons from which recordings were made, calcium transients were detected during blank periods at a rate of 0.09 ± 0.01 Hz (mean ± SEM., $n = 5$ animals, 77 neurons), with rates for individual cells up to 0.56 Hz. This is consistent with previous reports of low spontaneous firing rates in L2/3 visual cortex by using imaging in awake and anesthetized rats (8) and with extracellular recordings in anesthetized mice (25). When at least one monitor was viewed, the transient rate doubled to 0.18 ± 0.02 Hz, with individual rates up to 1.02 Hz (Fig. 4*C*). In 29% of neurons (22 of 77), a significant increase in the rate of Ca^{2+} transients was observed during viewed periods. ($P < 0.05$, Wilcoxon rank sum test). This difference was not due to contamination of the fluorescence signal by stimulation light (see *SI Text*).

Some neurons showed Ca^{2+} transients preferentially when the animal's gaze was directed at a specific monitor (Fig. 4 *D–F*). To analyze in more detail the relationship between Ca^{2+} transients and the orientation of the animal's head toward specific monitors, we first identified periods when only one monitor was within the ±45° region around the forward direction and occupied at least 400 square degrees within this region. We then determined the Ca^{2+}-transient rates for neurons when the animals head position satisfied these criteria for at least 10 s for each of the three monitors (Fig. 4*E*, $n = 35$ neurons). Seven of these 35 neurons (20%) showed a significantly higher rate for one monitor than the others ($P < 0.05$, Kruskal–Wallis test). In some cases, neighboring neurons preferred different monitors (Fig. 4 *E* and *F*).

This demonstrates that the head-mounted fiberscope can record functional signals with single-soma resolution in cortical layer 2/3 cells during exploratory behavior. The fiberscope is light enough so as to not restrict normal animal behavior, and even when the animal was moving vigorously, the strongest movement-based image shifts were mostly <3 μm. We show here that it is possible to image the responses of cortical neurons when the animal's interaction with the environment is self-determined, which occurs during natural behavior. We envisage that the main use of fiberscope imaging will be during behavioral tasks such as social behaviors, prey capture, behaviors involving vestibular stimulation, and interaction with physical objects.

Materials and Methods

Animal Preparation and Staining Procedures. All animal procedures were conducted according to the animal welfare guidelines of the Max Planck Society. Male Listar Hooded rats, weighing between 50 and 100 g at the time of first surgery, were used in the current study. During all surgical procedures, the animal's body temperature was maintained at 37°C by using a heating blanket and a thermal probe. At the end of each procedure animals were given flunixin-meglumin (1.5–2 mg/kg, s.c.; Finadyne) for postoperative analgesia. A small custom-built plate suitable for stabilizing the animal's head under a conventional two-photon microscope and onto which the fiberscope could also be attached was first implanted over the occipital region of the left cortical hemisphere under ketamine/xylacine anesthesia (ketamine from WDT; xylacine (Rompun) from Bayer) as described previously (8). During the implantation surgery, the approximate location of the primary visual area (λ + 2.5 mm, lateral 4 mm) was marked on the surface of the skull. At the end of this procedure, the exposed skull was covered by protective tape, and the animal was allowed to recover. Over the following 3 days, animals were habituated to head fixation in the experimental setup as described previously in ref. 8. After habituation, animals were anesthetized with isoflurane (Forene, 1.5–2%; Abbott), and an ≈4 × 4-mm area of skull was thinned until it was transparent when covered with saline solution. At the end of this procedure, the thinned skull area was covered with silicone and a glass coverslip, all exposed areas were closed again with protective tape and the animal was allowed to recover. Twenty-four to 72 h later, animals were sedated with ketamine (100 mg/kg), and the area of thinned skull was exposed, cleaned, and covered with saline solution. The location of the binocular primary visual area was then identified by using standard optical intrinsic signal imaging (see ref. 29). Briefly, excitation light was 630 ± 30 nm, individual trials were 6 s long (100-ms frame duration), 2-s prestimulus, 4-s stimulus; "blank" trials were interleaved with stimulated trials; a total of 40 trials comprised one imaging block. Imaging blocks were conducted for two different stimulus types, respectively, a bar (white on black background, 2.4° wide) moving (at 11°/s) vertically and horizontally. Care was taken to shield the optical system from the stimulus light. At the end of the intrinsic imaging session, the thinned skull area was again covered with silicone and a glass coverslip, the area closed and protected and animals returned to their home cage to recover. Twelve to 72 h later, animals were anesthetized with isoflurane (1.5–2%) and given furosemid (Lasix, 1.5–2 mg/kg, i.m.; Aventis) to reduce cortical swelling. An opening of ≈1 × 2 mm was made in the thinned bone over the identified visually responsive spot and the dura was removed. Staining of astrocytes was then performed by using Sulforhodamine 101 (Sigma–Aldrich) as previously described (21), before covering the craniotomy with agar and a glass coverslip. At the end of the procedure, animals were returned to their home cage and allowed to rest for at least 60 min. During this time, animals usually recovered consciousness after 3–5 min, resumed exploratory behavior within the cage, and regained appetite, as judged by animals eating Froot Loops (Kellogg's) or rat chow. After recovering, animals were head-fixed, and cells in the identified visually responsive area were located by using SR101 as a counterstain. The cell-permeable Oregon Green 488 BAPTA-1 acetoxymethyl ester (OGB-1 AM) was synthesized as described previously (US patent 6,162,931), purified to >99% via normal- and reversed-phase chromatography, and injected as described previously (5, 6). After OGB-1 loading, the objective unit (4 and 5, Fig. 1*A*) of the head-mounted fiberscope was carefully positioned over the loaded area (using the same lens setup as in the head-mount microscope but with a crosshair in place of the fiber-tip of the scanner). The scanner was the replaced and the animal taken to the recording arena.

Behavioral Environment and Stimulation. The arena for imaging in freely moving animals consisted of a semicircular track (radius ≈50 cm) with platforms (15 × 15 cm^2) at each end facing stimulation CRT monitors (see Fig. 3*A*). An additional CRT monitor was located at the center of the semicircle parallel to the track and opposite the other monitors. The stimulus was a static pattern of 6-cm-wide blue bars on a black background. Contrast was 100%, and average luminance for all monitors was 5.5 cd/m^2. Bar orientation on the monitor at the center of the track was vertical (0°) and, for the monitors at the ends of the track, 45° and −45°. The patterns were presented constantly while the animal moved around on the track. For imaging in anesthetized animals, a moving bar stimulus (8.7° wide, 8.7°/s), displayed on a single monitor, was presented 20 times during a continuous recording period with an interstimulus interval of 10 s.

Two-Photon Imaging. A Ti:Sapphire laser (MaiTai HP; Spectra-Physics) provided near-infrared laser pulses at 925 nm with an average power of 1.6 W. The beam intensity was controlled by using a Pockels cell (Model 350-80, Conoptics; Polytech). To compensate for the group velocity dispersion, the pulses were prechirped by using two prism arrays (10-prism sequence) as previously described (16). The beam was coupled to the polarization-maintaining excitation fiber (F-SPF; Newport) by an achromatic lens ($f = 18$ mm, achromat, 12 × 18 NIR-II; Edmund Optics) and a fiber launch (Thorlabs). A Faraday isolator (Linos) was used to block back reflections from the polarization-maintaining fiber as it was cleaved at 0°. The objective lens located within the microscope was custom designed (water-immersion, N.A. = 0.9, focal length 3 mm, working distance 0.7 mm; Throl Optische Systeme) and pressed into a sleeve that threads into a bushing, providing manual focus control. The main head-mount body contained the tube lens (achromat, $f = 12.7$ mm, LAKN22-SFL-6; Thorlabs) and provided the mounting surface for the dichroic splitter (2b; Calflex-X). A folding mirror (Calflex-X) was used between tube lens and scanner. The emitted fluorescence was concentrated onto a plastic optical fiber (POF, N.A. of 0.63, outside diameter 1 mm, PJU-FB1000; Thoray) with a condenser lens ($f = 9$ mm, f_SIL, VF082c; Pörschke). Fluorescence was then transmitted to photomultipliers (H7422P-40MOD, Hamamatsu) via the POF. The red and green channels were separated with dichroic mirrors (red: HQ610/75M at 18°, green: HQ535/50M-2P at 18°, Chroma Technology). The scanner was driven by a triangular signal on the fast (*x*) axis and a ramp-shaped signal on the slow (*y*) axis. Both signals were filtered by using Bessel filters (900C9L8L; Frequency Devices). Filtering affects the slow (*y*) drive signal only little, except for the fly back, but results in an essentially sinusoidal drive voltage in the fast (*x*) direction. Image distortions due to the excitation of fiber resonances were minimized by filtering below the fundamental frequency (≈700 Hz) (16). For functional measurements with the fiberscope, we used 64 × 64-pixel frames with either a 1.89-ms line duration and an 8.2-Hz frame rate or a 1.43-ms line duration and a 10.9-Hz frame rate. All freely moving animals were recorded at 10.9 Hz. Time course measurements on the conventional microscope used 64 × 128-pixel frames with 1.5-ms line duration (10.4-Hz frame rate).

Data Analysis. ***Quantification of brain movements.*** The magnitude of brain displacements in each imaging frame **t** was calculated by using the intraframe radial variance for each frame **t**:

$$r_i = \sqrt{\mathrm{Var}_j(x_{i,j}) + \mathrm{Var}_j(y_{t,j})}\,,$$

where $x_{t,j}$ and $y_{t,j}$ denote horizontal and vertical components of the jth estimate of image displacement vector for the tth frame.

Animal tracking and pose estimation. To determine the animal's position and its pose in three dimensions, we used videography to track the position of four LEDs affixed to the fiberscope. The positions of the LEDs were measured in three dimensions by using a micrometer (IP 65; Gant). The camera (DCR-TRV; Sony) operated at 29.97 Hz, 720 × 480 resolution, and 8-bit ''night vision'' mode was activated. The camera was first calibrated by using Tsai's camera model (30) by identifying in the video image 38 calibration points whose physical locations had been measured in three dimensions. Calibration produced the following parameters: location and orientation of the camera relative to the set of calibration points, the focal length in pixels, the aspect ratio of a single pixel, the location of the optical center in the image plane relative to the center of the digital image, and the lens distortion coefficient.

For each video frame n we denote by I_n the average of the grayscale values from the three color channels. We first calculated an image mask, consisting of those pixels that were at least 50 grayscale values higher than the median of In over all video frames. We next calculated an ''error image'' of the same size as I_n, with each pixel value corresponding to the evaluation of an error function indicating how unlikely it is for an LED center to reside at that pixel. The error image at a given pixel a in the image mask was defined as

$$E(a) = \sum_{b|D(a,b)\le r} \min(200,\ \max(0,250 - I_n(b))) \cdot \left(1 - 0.9\,\frac{D(a,\,b)}{r}\right),$$

where $D(a,b)$ is the distance in pixels between pixels a and b, and $r = 2$ is the radius of an LED in pixels. For pixels not in the image mask, $E(a)$ was set to the maximum possible value.

We then proceeded to estimate the rigid motion (translation followed by rotation) that maps the measured 3D positions of the four LEDs into their true coordinates relative to the camera. Given a candidate for such a motion, consisting of offsets and Euler angles, we can project each of the LEDs onto the video frame by using the parameters obtained from the camera calibration. Summing E over the location of the four LEDs thus gives rise to an error function to be minimized with respect to the parameters of the rigid motion. For details of the algorithm used, see *Animal Tracking and Pose Estimation* in *SI Text*. We also determined the 3D position and orientation of each CRT screen relative to the camera by measuring its width and height, marking the bottom corners as well as the left, right, and top edges of the screen in the video image and minimizing the reprojection error.

The previous procedures allowed us to determine the location of the four LEDs and three screens in three dimensions. We then defined a coordinate system based on forward, right, and up relative to the animal's head. The first axis (''forward'') was defined by the direction of a laser pointer when mounted below the fiberscope, the second axis (''up'') was taken to be as close as possible to the vertical axis of the fiberscope while still remaining at a right angle to the forward vector, and the third axis (''animal's right'') was automatically determined based on orthogonality to the two other axes. Given these rectangular coordinates for a point p, we defined spherical coordinates as follows. The vertical angle (''latitude'') was defined as $\sin^{-1}(p_3/|p|)$, whereas the horizontal angle (''longitude'') was defined as $\tan^{-1}(p_2/p_1)$. We then calculated the area on the unit sphere occupied by each screen, considering only the region within 45° of the forward axis in both vertical and horizontal angles. This area is then the ''solid angle'' subtended by the monitor in the given region of spherical coordinates in steradians, which we converted to square degrees.

Analysis of Orientation and Monitor Selectivity. To compare neural activity recorded with the fiberscope under various conditions, we applied parametric ANOVA tests to $\Delta F/F_0$ values or nonparametric Kruskal–Wallis tests to the counts of detected calcium transients. We determined which neurons responded to sensory stimulation and which showed orientation/direction selectivity as described in ref. 7. Mean fluorescence values ($\%\Delta F/F_0$) were calculated over a 2.5-s window after each stimulus as well as during null periods in which the stimulation screen was blank. For each neuron, an ANOVA was performed over all stimulation angles as well as blank periods, and neurons with p-values less than 0.01 were identified as visually responsive. In visually responsive neurons, a second ANOVA was performed over all stimulation angles, and $P < 0.01$ was used as the threshold for angular tuning. We also used the rate of detected Ca^{2+} transients over the same 2.5-s window to calculate the proportion of responsive neurons (29%, $P < 0.05$, Kruskal–Wallis tests) and the proportion of responsive neurons classified as selective for stimulus angle (83%); these results were not significantly different from those obtained by using mean $\Delta F/F_0$ values ($P > 0.05$, Fisher's exact t test) All analyses and statistical tests were implemented in Matlab (Mathworks).

ACKNOWLEDGMENTS. We thank Michael Müller, Jürgen Trutthardt (Max Planck Institute, Heidelberg), Stefan Weber, Karl-Heinz Hofmann, and Steffen Baier (Max Planck Institute, Tübingen) for outstanding technical help and fabrication of microscope components, as well as Luke Lavis for synthesis and purification of OGB1. We also thank Arno Schmitt, Verena Pawlak, Vishnudev Ramachandra, Elizabeth Hopp, Uwe Czubayko, and Jonas Kosten for help with data processing. This work was supported by the Max Planck Society.

1. O'Keefe J, Dostrovsky J (1971) The hippocampus as a spatial map. Preliminary evidence from unit activity in the freely-moving rat. *Brain Res* 34171–175.
2. Taube JS, Muller RU, Ranck JB, Jr (1990) Head-direction cells recorded from the postsubiculum in freely moving rats. I. Description and quantitative analysis. *J Neurosci* 10:420–435.
3. Hafting T, Fyhn M, Molden S, Moser MB, Moser EI (2005) Microstructure of a spatial map in the entorhinal cortex. *Nature* 436:801–806.
4. Denk W, Strickler JH, Webb WW (1990) Two-photon laser scanning fluorescence microscopy. *Science* 248:73–76.
5. Kerr JN, Greenberg D, Helmchen F (2005) Imaging input and output of neocortical networks in vivo. *Proc Natl Acad Sci USA* 102:14063–14068.
6. Stosiek C, Garaschuk O, Holthoff K, Konnerth A (2003) In vivo two-photon calcium imaging of neuronal networks. *Proc Natl Acad Sci USA* 100:7319–7324.
7. Ohki K, Chung S, Ch'ng YH, Kara P, Reid RC (2005) Functional imaging with cellular resolution reveals precise micro-architecture in visual cortex. *Nature* 433:597–603.
8. Greenberg DS, Houweling AR, Kerr JN (2008) Population imaging of ongoing neuronal activity in the visual cortex of awake rats. *Nat Neurosci* 11:749–751.
9. Kerr JN, et al. (2007) Spatial organization of neuronal population responses in layer 2/3 of rat barrel cortex. *J Neurosci* 27:13316–13328.
10. Sato TR, Gray NW, Mainen ZF, Svoboda K (2007) The functional microarchitecture of the mouse barrel cortex. *PLoS Biol* 5:e189.
11. Dombeck DA, Khabbaz AN, Collman F, Adelman TL, Tank DW (2007) Imaging large-scale neural activity with cellular resolution in awake, mobile mice. *Neuron* 56:43–57.
12. Chapin JK, Woodward DJ (1982) Somatic sensory transmission to the cortex during movement: gating of single cell responses to touch. *Exp Neurol* 78:654–669.
13. Lee AK, Manns ID, Sakmann B, Brecht M (2006) Whole-cell recordings in freely moving rats. *Neuron* 51:399–407.
14. Helmchen F, Fee MS, Tank DW, Denk W (2001) A miniature head-mounted two-photon microscope. High-resolution brain imaging in freely moving animals. *Neuron* 31:903–912.
15. Piyawattanametha W et al. (2006) Fast-scanning two-photon fluorescence imaging based on a microelectromechanical systems two-dimensional scanning mirror. *Opt Lett* 31:2018–2020.
16. Sawinski J, Denk W (2007) Miniature random-access fiber scanner for in vivo multiphoton imaging. *J Appl Phys* 102:034701.
17. Engelbrecht CJ, Johnston RS, Seibel EJ, Helmchen F (2008) Ultra-compact fiber-optic two-photon microscope for functional fluorescence imaging in vivo. *Opt Exp* 16:5556–5564.
18. Flusberg BA, et al. (2008) High-speed, miniaturized fluorescence microscopy in freely moving mice. *Nat Methods* 5:935–938.
19. Jung JC, Mehta AD, Aksay E, Stepnoski R, Schnitzer MJ (2004) In vivo mammalian brain imaging using one- and two-photon fluorescence microendoscopy. *J Neurophysiol* 92:3121–3133.
20. Levene MJ, Dombeck DA, Kasischke KA, Molloy RP, Webb WW (2004) In vivo multiphoton microscopy of deep brain tissue. *J Neurophysiol* 91:1908–1912.
21. Nimmerjahn A, Kirchhoff F, Kerr JN, Helmchen F (2004) Sulforhodamine 101 as a specific marker of astroglia in the neocortex in vivo. *Nat Methods* 1:31–37.
22. Miyawaki A, et al. (1997) Fluorescent indicators for Ca^{2+} based on green fluorescent proteins and calmodulin. *Nature* 388:882–887.
23. Xu C, Webb WW (1996) Measurement of two-photon excitation cross sections of molecular fluorophores with data from 690 to 1050 nm. *J Opt Soc Am B* 13:481–491.
24. Girman SV, Sauve Y, Lund RD (1999) Receptive field properties of single neurons in rat primary visual cortex. *J Neurophysiol* 82:301–311.
25. Niell CM, Stryker MP (2008) Highly selective receptive fields in mouse visual cortex. *J Neurosci* 28:7520–7536.
26. Kleinfeld D, Mitra PP, Helmchen F, Denk W (1998) Fluctuations and stimulus-induced changes in blood flow observed in individual capillaries in layers 2 through 4 of rat neocortex. *Proc Natl Acad Sci USA* 95:15741–15746.
27. Greenberg DS, Kerr JN (2009) Automated correction of fast motion artifacts for two-photon imaging of awake animals. *J Neurosci Methods* 176:1–15.
28. Schummers J, Yu H, Sur M (2008) Tuned responses of astrocytes and their influence on hemodynamic signals in the visual cortex. *Science* 320:1638–1643.
29. Grinvald A, Lieke E, Frostig RD, Gilbert CD, Wiesel TN (1986) Functional architecture of cortex revealed by optical imaging of intrinsic signals. *Nature* 324:361–364.
30. Tsai RY (1992) A versatile camera calibration technique for high-accuracy 3D machine vision metrology using off-the-shelf TV cameras and lenses. *IEEE J Robotics Automation RA*-3:323–344.